HHS Public Access

Author manuscript

Acta Biomater. Author manuscript; available in PMC 2015 October 01.

Published in final edited form as:

Acta Biomater. 2014 October ; 10(10): 4323–4331. doi:10.1016/j.actbio.2014.06.034.

Engineering alginate as bioink for bioprinting

Jia Jia[1,†], **Dylan J. Richards**[1,†], **Samuel Pollard**[1], **Yu Tan**[1], **Joshua Rodriguez**[1], **Richard P. Visconti**[2], **Thomas C. Trusk**[2], **Michael J. Yost**[2], **Hai Yao**[1,2], **Roger R. Markwald**[2], and **Ying Mei**[1,2,*]

[1]Bioengineering Department, Clemson University, Clemson, SC 29634, USA

[2]Department of Regenerative Medicine and Cell Biology, Medical University of South Carolina, Charleston, SC 29425, USA

Abstract

Recent advances in 3D printing offer an excellent opportunity to address critical challenges faced by current tissue engineering approaches. Alginate hydrogels have been extensively utilized as bioinks for 3D bioprinting. However, most previous research has focused on native alginates with limited degradation. The application of oxidized alginates with controlled degradation in bioprinting has not been explored. Here, we prepared a collection of 30 different alginate hydrogels with varied oxidation percentages and concentrations to develop a bioink platform that can be applied to a multitude of tissue engineering applications. We systematically investigated the effects of two key material properties (i.e. viscosity and density) of alginate solutions on their printabilities to identify a suitable range of material properties of alginates to be applied to bioprinting. Further, four alginate solutions with varied biodegradability were printed with human adipose-derived stem cells (hADSCs) into lattice-structured, cell-laden hydrogels with high accuracy. Notably, these alginate-based bioinks were shown to be capable of modulating proliferation and spreading of hADSCs without affecting structure integrity of the lattice structures (except the highly degradable one) after 8 days in culture. This research lays a foundation for the development of alginate-based bioink for tissue-specific tissue engineering applications.

Keywords

Oxidized Alginate; Adipose-derived stem cells; Bioink; Hydrogel scaffold; Bioprinting

*Corresponding author: mei@clemson.edu; FAX - (843) 876-2416.

†These authors contributed equally to this work

1. Introduction

3D bioprinting provides a rapid and robust approach to fabricate functional tissues *in vitro* [1–6]. To facilitate tissue formation, alginates have been extensively utilized as bioink to provide a matrix scaffold to direct a specific 3D cell growth because it can robustly form cell-compatible hydrogels in physiological conditions. In addition, it can be modified for a variety of tissue engineering applications, including bone, vascular, and adipose tissue engineering [7–18]. However, native alginate is a bioinert material (i.e., lack of cell-adhesive moieties) with limited biodegradation [4,9,12]. Mooney and coworkers have shown that chemical modification of alginate through oxidation allows for controlled degradation [19–21]. Due to this desirable characteristic for tissue engineering applications, oxidized alginate holds great potential as ink for bioprinting. However, little previous research has explored the applications of oxidized alginates in bioprinting.

In this study, we prepared a library of 30 different alginate solutions with varied oxidation percentages and concentrations to develop a tunable bioink platform for bioprinting that can be modified for a wide range of tissue engineering applications. To this end, we have analyzed two key physical properties (i.e., viscosity and density) for the alginate solutions in the library and systematically investigated the effects of those physical properties of the alginates on their printability using a piston-driven, liquid-dispensing system and human adipose-derived stem cells (hADSCs). hADSCs were selected in this study because of their high proliferation rates, a persistent multipotency, and a well characterized morphology in 2D culture [24]. This has allowed for the identification of a suitable range of material properties of alginates for bioink development. Further, the alginate-based bioinks were shown to be capable of modulating important stem cell behavior, such as proliferation and spreading, without affecting their printability and structural integrity after 8 days in cell culture (Fig. 1). The research reported here will accelerate the development of alginate-based bioink for tissue-specific tissue engineering applications.

2. Materials and methods

2.1 Materials

Sodium alginate was purchased from FMC BioPolymer (Philadelphia, PA). Ethylene glycol was purchased from Mallinckrodt Baker, Inc. (Phillipsburg, NJ). All other chemicals used for this study were purchased from Sigma-Aldrich (St. Louis, MO) unless otherwise stated.

2.2 Alginate synthesis and oxidation

Sodium alginate was prepared using the method established by Bouhadir and others [20]. Briefly, 1 g sodium alginate was dissolved in 100 mL of distilled water. Sodium periodate was used as the oxidizing reagent and was added at room temperature in varying quantities, based on the desired percent oxidation (at oxidation percentage of 1%, 3%, 5%, 10%, w/w). The reaction was terminated by the addition of ethylene glycol after 24 hours. Sodium chloride (3 g) was then dissolved in the solution. Excess amount of ethyl alcohol was added to the solution (2:1 ratio), precipitating the oxidized alginates. The solution was centrifuged to collect the precipitates, and the ethanol wash was repeated. The oxidized alginate pellets were then lyophilized and stored at −20°C.

2.3 RGD-alginate conjugation

To promote cell attachment and spreading, RGD peptides have been conjugated into oxidized alginates using a similar method as Mooney's group, reported in Rowley et al. 1999: utilizing aqueous carbodiimide chemistry with G_4RGDSP-OH (International Peptides, Louisville, KY) [9]. The final modification percentage of RGD to alginate was 1% (w/w).

2.4 Identification of viscosity and density

Aqueous alginate solutions (at oxidation percentage of 0%, 1%, 3%, 5%, 10% w/w) of varying concentration (2%, 5%, 8%, 10%, 15%, 20% w/w) were made using a weight to total-weight ratio. To test viscosity, approximately 8 mL of varying alginate solutions were made and tested three times by Cannon-Fenske Opaque Calibrated viscometers (Cannon® Instrument Company, Inc, USA) at 40 °C. Viscosity values were calculated according to Poiseuille's law associated with the calibrated viscometers and then converted to kinematic viscosities by dividing by density. The density of the alginate solutions were calculated by measuring the mass of 1 mL of alginate aqueous solution three times and then averaged.

2.5 Preparation of Ca^{2+}-containing gelatin substrate for 3D-printing alginate hydrogels

To avoid reduced viability with high Ca^{2+} concentration solutions, a calcium substrate was prepared for alginate, as done previously [25]. Briefly, a 100 mM $CaCl_2$ gelatin solution was prepared by combining calcium chloride dehydrate, sodium chloride (0.9 wt%), and porcine gelatin (2 wt%) in distilled water and boiled for 2 minutes. Aliquots of 5 mL of gelatin were put into standard petri dishes to gel in a refrigerator overnight. Titanium dioxide (0.3% wt%) was added to the same solution and stirred for 10 min to increase the opacity of the resulting surface. 3 mL of the gelatin/TiO_2 mixture was spread evenly across the surface of the previously prepared gelatin plates and put in the refrigerator overnight to be used within 3 days.

2.6 Printing process of alginate hydrogels

Aqueous alginate samples were prepared according to a weight to total-weight ratio using either distilled water (for density and viscosity tests) or cell medium (for dot analysis and cell studies) using the same preparation protocol. The bioink (with cells for cell study) were then loaded into a printer-compatible syringe. All printing was performed on the Palmetto Printer, a custom-made, piston-driven deposition system, on a temperature-controlled plate at 4 °C. Droplet volume was maintained at 230 nL with a dispensing speed of 10 μL/sec.

For dot analysis, a 5×5 dot array was printed for each sample and left to gel for 40 min before macroscopic imaging with the Olympus SZX16 stereomicroscope.

For lattice structure fabrication, single layer, cell-laden, lattice structures were printed with 7 columns and 7 rows using a point-to-point strategy to print every other dot with optimal expected dimensions of 12.6 mm x 12.6 mm (X, Y), which is a result of a printing design with dimensions of 12 mm × 12 mm (from the center of dot placement) (Fig. 3a and Supplementary Video 1). In liquid-dispensing printing, the point-to-point method allows for accurate control of design-specific structures. The bioink used for the structures were alginate solutions of 0% ox.-8% conc., 5% ox.-10% conc., 5% ox.-15% conc., 5% ox.-20%

conc., 10% ox.-15% conc. Following printing, 8 mL of media was added to the gelatin plate and put in the incubator for approximately 30 min, melting the Ca^{2+}-containing gelatin to maximize alginate crosslinking. Lattice structures were then transferred to individual wells in a 6-well plate for extended culture. Macroscopic pictures were taken with the Olympus SZX16 stereomicroscope, and media was changed every 4 days for 8 days.

2.7 Cell culture and cell behavior studies

Human adipose-derived stem cells (hADSC) (Lonza, Basel, Switzerland) were used to investigate the effects of the alginate gel's oxidation and concentration on cell viability, attachment, and proliferation. The cells were cultured in low glucose DMEM with 10% FBS and 1% penicillin-streptomycin, 1% glutamine, and 1% antimycin (Gibco Life Technologies, Grand Island, NY). At >80% confluency, cells were detached using trypLE Express (Gibco Life Technologies) and passaged. All experiments were conducted using passage 5 (P5) hADSCs. Aqueous alginate solutions of varying oxidation and concentration were prepared using the cell culture medium and mixed with detached cells at a concentration of 1.3 million cells per mL. The samples were loaded into printer syringes, transported to the printer, and then printed as described in the previous section.

hADSC suspension tests were performed by mixing aqueous alginate samples (made with media) of varying concentrations with live cells (1 mL of 1.3 million cells per mL) labeled with Calcein, AM (Gibco Life Technologies). The samples were loaded into NMR tubes and were left stationary for 3 hours. Then, each solution was partitioned from top to bottom into 5 parts, and the number of cells in each part was counted microscopically and analyzed. The macroscopic images were taken with the Olympus SZX16 stereomicroscope.

The cell-seeded hydrogels were assessed for cell viability post-printing using the live/dead cell viability assay kit from Invitrogen Life Technologies (Grand Island, NY) following the protocol of the kit. The cell viability percentage was calculated as the number of live cells (green-stained) over the total number of cells (green and red). Viability assays were performed for the printed structures again after 8 days of culture using portions of each structure. High viscosity samples of each oxidation (0% ox.-10% conc., 1% ox.-10% conc., 3% ox.-15% conc., 10% ox.-20% conc.) were later tested using the same post-printing method. All the fluorescent pictures were taken by Leica TCS SP5 AOBS Confocal Microscope System.

The lattice structures of five samples (0% ox.-8% conc., 5% ox.-10% conc., 5% ox.-15% conc., 5% ox.-20% conc., 10% ox.-15% conc.) were printed with hADSCs following the protocol above. Cell proliferation and morphology for these samples were assessed at day 0, day 4, and day 8 using portions of each structure with a fluorescent DAPI and phalloidin staining kit from Invitrogen Life Technologies (Grand Island, NY) by following the kit protocol. For cell proliferation analysis, the following cell counting method was utilized on each of the given days. At least 3 different pictures (600 μm × 600 μm, z-layer thickness ≈ 100 μm) were taken of the respective hydrogel samples, and the cell number in 3 random areas (200 μm × 200 μm, >10 cells/area) of each picture were manually counted based on DAPI and phalloidin staining. Proliferation index was calculated as the cell number of each day of each sample divided by the original cell number on day 0 for the 0% ox.-8% conc.

alginate sample. For cell morphology, fluorescent images of each sample (at least 4 random pictures per sample, 600 μm × 600 μm per picture) were taken by the Leica TCS SP5 AOBS Confocal Microscope System using Z-stack parameters of 30 optical slices over a 300 μm depth. Cell sizes were measured through ImageJ threshold-based edge detection tools as a total cell area divided by the number of cells normalized over the values at day 0 for the 0% ox.-8% conc. alginate sample (Fig. 4c). The cell-matrix interactions between hADSCs and alginates were studied using mouse primary antibody for $\alpha_v\beta_3$ integrin (Abcam, Cambridge, MA) and rat (anti-mouse) secondary antibody, Alexa Fluor 546 (Invitrogen, Carlsbad, CA), both at 1:200 ratio.

2.8 Rebuilt 3D image for printed lattice structure

The cells in the printed lattice structure were stained with fluorescently labeled phalloidin and imagined by Leica TCS SP5 AOBS Confocal Microscope System. These images were rebuilt into a 3D rendering using Amira software.

2.9 Statistical analysis

The results were expressed as the mean ± standard deviation (SD) and analyzed using JMP 11 and Excel statistical software. Lattice dimensions were compared between day 0, day 4, and day 8 by a Student's *t*-test. Dot analysis, viscosities, and densities were analyzed separately using unpaired Student's *t*-tests. A confidence interval of 95% was used.

3. Results and Discussion

Alginate has been widely used as a cell encapsulation material and in tissue engineering scaffolds [7,26]. However, native alginate is a bio-inert material with limited biodegradation. To improve this, Mooney's group introduced a controllable degradation process using oxidized alginates reported in Bouhadir et al. 2001, which showed a promising capability as scaffold for tissue engineering applications [19,20,27]. These biodegradable alginates thus have great potential to develop a bioink platform for 3D bioprinting.

In 3D printing, there are multiple, unique dispensing systems to achieve high resolution, and each system has specific requirements for the optimal ink [28]. Among the various liquid-dispensing systems, piston-driven deposition has recently received significant attention because it offers a significantly high fabrication speed and is capable of fabricating anatomically shaped, clinically relevant-sized constructs [29,30]. They require a bioink with a suitable density and viscosity as well as the capability to retain printing fidelity and high cell viability post-printing [31,32]. In this study, we used a custom-made, piston-driven deposition system, as a test bed to examine the printability of biodegradable alginates. The printability here is defined as having high printing resolution and fidelity, a homogeneous cell distribution, and high cell viability post-printing [23]. In addition, a lattice structure was utilized as our standard to evaluate printing resolution and fidelity in this study because it has been shown to promote cell viability and cell function (i.e. proliferation), offering the possibility of long-term culture *in vitro* without the assistance of a bioreactor [33].

Initial efforts focused on the oxidized alginate previously utilized for tissue engineering applications, such as 5% ox.-2% conc. (i.e., alginate with 5% oxidation and 2% (w/w)

concentration) [20]. However, these alginate solutions did not provide sufficient printing resolution for a lattice structure due to its low viscosity (Fig. 3b, *top*). Also, alternating the oxidization percentage between 0% (non-degradable), 1%, 3%, 5%, and 10% proved to be inadequate to increase resolution for a 2% concentration solution. Meanwhile, other reported attempts to increase resolution while maintaining high cell viability in literature have used higher concentrations [33]. Therefore, a range of concentrations (2%, 5%, 8%, 10%, 15%, and 20%) mixed with different oxidation levels was designed to create a library composed of 30 different alginates (Fig. 2). Using the three criteria for printability evaluation (i.e., homogenous cell distribution, high printing resolution, and high cell viability post-printing) [22,23,33,34], we systematically examined the material properties and printability of these alginates with hADSCs as a model cell line using a piston-driven, liquid-dispensing system.

3.1 Density and cell suspension tests of different alginate solutions

Homogeneity of cell distribution after printing is critical for the ideal bioink. To achieve a homogeneous cell suspension throughout the whole printing process, the density of the biomaterial should be close to or above that of the examined cell type [35]. By altering oxidation and concentration, a matrix of alginate densities was made (Fig. 2a). With increasing concentration and decreasing degree of oxidation, the densities of alginates showed an increasing trend. Given a printing operation time of 3 hours, we identified the range of materials that keep cells homogenously distributed for printing with a piston-driven deposition system (Fig. 2a, *green*), which was verified by fluorescently labeled cell suspension tests (Fig. 2b). The results of this experiment and density measurements of all 30 materials confirm that a density around 1.05 g/cm^3 can maintain a homogeneous cell suspension for hADSCs. This is in agreement with the study by Lin and others that optimized a polyethylene glycol (PEG)-based hydrogel with 37.5% Percoll to attain the needed density to suspend hADSCs [35]. Density, thus, can define a limit for bioprinting alginate solutions. The individual cell density and biomaterial density must be taken into account when applying a density-based selection to other systems. It is important to note that a wider range of densities around 1.05 g/cm^3 can maintain a hADSC suspension within a 3 hour printing process time without significant cell movement, due to the relatively high viscosity that slows the process of cell movement.

3.2 Viscosities of 30 different alginate solutions

Given that viscosity plays an important role in a liquid-dispensing printer [28], its effects on printability (i.e., printing resolution) were examined to determine a viscosity-based range for oxidized alginate ink. We found that altering oxidation and concentration resulted in a practical method of controlling the viscosity of degradable alginates. A similar pattern to the density measurements was observed: as the concentration increased or the degree of oxidation decreased, the viscosity showed an increasing trend (Fig. 3a). In addition, we have printed 5×5 arrays of dots using different biodegradable alginates to examine the effect of viscosity on dot fidelity and size, which determines printing resolution. As shown in Figure 3b and Figure 3c, there is an optimal range of viscosity (i.e., ~200 mm^2/s to ~3000 mm^2/s) for the improved printing resolution independent of concentration and oxidation degree of alginate solution. This indicates the critical role of viscosity in printing resolution for a piston-driven, liquid-dispensing system. At the low viscosity end (i.e., <200 mm^2/s), low

concentration alginates produced larger dots when compared with alginates within the optimal range of viscosities (Fig. 3c). On the other hand, an upper threshold (i.e., >3000 mm^2/s) also exists due to the increased liquid handling difficulty after a certain viscosity value (Fig. 3c). It is known that high viscosity can alter liquid-dispensing characteristics of the solution. For example, Schuurman and coworkers reported that high viscosity materials can form filaments rather than droplets when depositing [36]. Notably, alginate solutions with viscosities between ~200 mm^2/s and ~400 mm^2/s typically had densities lower than the threshold necessary for maintaining homogenous cell suspension (i.e., <1.05g/mL). The viscosity range suitable for high printability was therefore refined to ~400 mm^2/s to ~3000 mm^2/s. The alginate solutions within the optimal range of viscosity are highlighted in green in Figure 3a. The data presented in Figure 3a will enhance the available viscosity data on alginates used in other bioink development research with liquid-dispensing systems [37–39].

3.3 hADSC viability in the printed alginate

Cell viability, as one of the standards of biocompatibility for bioink, was analyzed after printing [22]. To examine the effect of printing on cells, viabilities were assayed immediately following the printing process (Figs. 4a and 4b). A compromised cell viability (<90%) was found in the high viscosity alginates (>3000 mm^2/s), while high cell viability (>90%) was found in the alginate solutions with the optimal/medium viscosity (~400 mm^2/s to ~3000 mm^2/s). The decreased cell viability in the high viscosity alginate samples was attributed to the limited nutrient transport (i.e., diffusivity). Viability assays were performed again after 8 days in cell culture, as shown in Figure 4c. The alginates with optimal/medium viscosity (i.e., ~400 mm^2/s to ~3000 mm^2/s) again exhibited high viability (>90%), whereas the alginates with high viscosity showed a negligible viability (0%). The results indicate that alginates with high viscosity, although printable, may create an environment with poor nutrient transport, resulting in compromised cell viability, in accordance with previous studies [40,41]. Given the importance of maintaining high cell viability post-printing, it is a key parameter to include when defining the range of engineered alginates for bioink.

3.4 Summary of the oxidized alginates based on three printability criteria

The capacity to maintain homogenous cell suspension (influenced by the densities of alginates samples) and achieving high printing resolution and viability (both influenced by the viscosities of samples) are the three criteria for our bioink selection. Based on these criteria, a new table was assembled to highlight the printable alginate solutions (Fig. 5). It is important to note that these highlighted alginates can serve as base materials to develop bioinks with desired physical/chemical/biological properties for tissue-specific tissue engineering applications [19]. Further, the density, viscosity, and viability analysis allowed for the identification of a suitable range of material properties of alginate solutions to be applied to bioprinting. This can provide a guideline for developing next generation of alginate-based bioink for 3D bioprinting-facilitated tissue engineering. Notably, Mooney and coworkers have demonstrated the independent control of elastic moduli and degradation rates of alginate hydrogels by creating binary alginate hydrogels [42].

3.5 Printing lattice-structured, cell-laden alginate hydrogels and cell culture

Lattice structures have been shown to support higher cell viability and proliferation rate because they offer a conducive environment for nutrient supply and waste excretion [33]. In this study, we designed a point-to-point protocol to produce cell-laden hydrogels with a lattice structure of 7 columns and 7 rows. They have optimal expected dimensions of 12.6 mm × 12.6 mm (X, Y) based on a printing design dimension of 12 mm × 12 mm (from the center of dot placement) and a Z dimension limited to one layer (Fig. 6a). To examine the effects of the biodegradability of oxidized alginate, we selected samples with low degradable (0% ox.), medium degradable (5% ox.), and high degradable (10% ox.) characteristics. The density, viscosity, and viability analysis allow for the selection of the appropriate concentrations for each alginate sample (0% ox.-8% conc., 5% ox.-10% conc., 5% ox.-15% conc., 10% ox.-15% conc.) to be printed with suspended hADSCs. Although these four materials have significant differences in their physical properties (i.e., density and viscosity) (Figs. 2 and 3), they all can be successfully printed into lattice-structured, cell-laden hydrogels with homogeneous cell distribution (Figs. 6 and 7a). Notably, the dimensions of all the printed lattice structures were within 10% of the optimal expected dimensions (i.e., 12.6 mm × 12.6 mm) (Fig. 6c), which can be defined as accurately printed structures [43].

All lattice structures were cultured for 8 days. For the samples that maintained measurable structures, the changes in length and width were measured at day 0, day 4, and day 8, and the extent of dimensional changes were determined (Fig. 6c). The 0% ox.-8% conc., 5% ox.-10% conc., and 5% ox.-15% conc. samples remained intact through 8 days in culture, and the rapid degradation of 10% ox.-15% conc. alginate resulted in almost complete fracture of the structure by day 8 [20]. Further, no significant change in dimension (Y dimension, $p=0.10$; X dimension, $p=0.27$) was observed in the 0% ox.-8% conc. sample from day 0 to day 8 (Fig. 6c), whereas a significant dimensional decrease (Y dimension, $p<0.05$; X dimension, $p<0.05$) was observed in the 5% ox.-10% conc. and the 5% ox.-15% conc. samples from day 0 to day 8. The decrease in dimension of the oxidized alginate samples was attributed to their biodegradation and cell activities. This consistent decrease should be considered, especially for dimension-specific designs when using dynamic or prolonged culture methods.

3.6 hADSC spreading and proliferation assays in printed lattice structures

In addition to maintaining cell viability, a bioink platform should allow for the modulation of cell behaviors. In this study, proliferation and spreading of hADSCs were examined due to their important roles in tissue engineering applications. In particular, cell spreading can be used to modulate self-renewal and differentiation of hADSCs [44–46]. Cell-adhesive RGD peptide, a widely known cell attachment promoter molecule [9,47–49], was conjugated to alginate bioink in this study to promote cell proliferation and spreading (Supplementary Fig. 1). DAPI staining for nuclei and phalloidin staining for actin were used to characterize the cell behavior in each structure (Fig. 7a). As shown in Figure 7a, 7b, and 7c, the oxidized alginate bioinks (i.e., 5% ox.-10% conc., 5% ox.-15% conc., and 10% ox.-15% conc. samples) can effectively promote cell proliferation and spreading when compared to the non-oxidized alginate bioink (i.e., 0% ox.-8% conc. alginate). Quantitatively, the cell

proliferation percentages after 8 days in culture were 173% for the 0% ox.-8% conc. alginate, 232% for the 5% ox.-10% conc. alginate, 248% for the 5% ox.-15% conc. alginate (Fig. 7b), and 190% for the 10% ox.-15% conc. alginate at day 4. For cell spreading, the average cell size did not change significantly after 8 days in culture for the 0% ox.-8% conc. alginate, while cell size increased 25% for the 5% ox.-10% conc. alginate, 161% for the 5% ox.-15% conc. alginate at day 8, and 69% for the 10% ox.-15% conc. alginate at day 4 (Fig. 7c). The low cell proliferation and cell spreading in the 0% ox.-8% conc. alginate assumed to be attributed to its persistent low porosity given its limited degradability. In contrast, the significant increase in cell proliferation and spreading in the 5% ox.-15% conc. alginate was assumed to be attributed to the increasing porosity associated with its degradation. The vast difference in cell spreading among alginate bioinks with varied oxidation degree and concentration (i.e., 0% ox.-8% conc., 5% ox.-10% conc., and 5% ox.-15% conc. samples) demonstrates their great potential in printing scaffolds tailored for specific tissue engineering applications. For example, the 0% ox.-8% conc. alginate induced a round cell morphology that can be applied to chondrogenesis, while the 5% ox.-15% conc. alginate was associated with an increased spreading phenotype that could facilitate osteogenesis [50–55]. In addition, the cell-matrix-interactions between hADSCs and alginates were investigated using $\alpha_v\beta_3$ integrin immunofluorescent staining as shown in Supplementary Figure 2. The RGD conjugation was found to promote integrin expression at all three dates (i.e., day 0, day 4 and day 8). Interestingly, the $\alpha_v\beta_3$ integrin expression was found on day 8 for alginate samples without RGD conjugation, which was attributed to the ECM secreted by hADSCs, consistent with previous research [56].

Figure 8 is a 3D picture showing a portion of a lattice structure from the 5% ox.-15% conc. oxidized alginate with hADSCs after 8 days in culture. The distribution of the observed spreading cells confirmed that the homogenous cell distribution in the alginate-based bioink pre-printing was maintained in the lattice structure after 8 days in cell culture. Summarizing the results shown in Figure 6 and Figure 7, the alginate-based bioinks are capable of modulating hADSC proliferation and spreading without affecting structural integrity after 8 days in culture, apart from the highly degradable alginate sample, 10% ox.-15% conc. This creates a solid foundation for the development of alginate-based bioink for 3D bioprinting-tailored tissue engineering scaffolds.

Conclusion

The primary characteristics influencing the printability of oxidized alginate as ink for bioprinting was defined by its ability to hold a homogeneous cell suspension, have high printing resolution, and support high cell viability. According to these factors, an ideal printable range for using oxidized alginate as a bioink platform was established. Further, these alginate-based bioinks were shown to be capable of modulating hADSC functions without affecting their printability and structure integrity after cell culture. The introduction of oxidized alginate to bioprinting has led to the creation of a tunable bioink platform for a range of tissue fabrications. Based on our findings, the observed functional relationship between the material properties (i.e., viscosity and density) of alginate and its printability allows for an enhanced progression in alginate bioink development for liquid-dispensing printing. When using other cell types, metabolic demands may require an altered density and

viscosity of oxidized alginate to allow for optimal diffusion of nutrients. Apart from diffusion limitations, the Ca^{2+} concentration used in the gelation process may also affect Ca^{2+}-sensitive cell types, such as chondrocytes [57]. This Ca^{2+} concentration can be adjusted to achieve higher viability, though a prolonged gelation time may affect the printing fidelity and total printing time [25]. Future studies in bioprinting technology and a widened understanding of self-assembly mechanisms between cells may reshape the demands for ink printability.

Supplementary Material

Refer to Web version on PubMed Central for supplementary material.

Acknowledgments

The work is supported by the National Science Foundation (NSF - EPS-0903795), the startup funds from Clemson University, and the National Institutes of Health (8P20 GM103444). This study used the services of the Morphology, Imaging and Instrumentation Core, which is supported by NIH-NIGMS P30 GM103342 to the South Carolina COBRE for Developmentally Based Cardiovascular Diseases. We would like to thank Agnes Nagy Mehesz for the support in cell culture. Joshua Rodriguez was supported by the NSF-REU program.

References

1. Visconti RP, Kasyanov V, Gentile C, Zhang J, Markwald RR, Mironov V. Towards organ printing: engineering an intra-organ branched vascular tree. Expert Opin Biol Ther. 2010; 10:409–420. [PubMed: 20132061]
2. Fedorovich NE, Alblas J, Hennink WE, Oner FC, Dhert WJA. Organ printing: the future of bone regeneration? Trends Biotechnol. 2011; 29:601–606. [PubMed: 21831463]
3. Mironov V, Kasyanov V, Markwald RR. Organ printing: from bioprinter to organ biofabrication line. Curr Opin Biotechnol. 2011; 22:667–673. [PubMed: 21419621]
4. Norotte C, Marga FS, Niklason LE, Forgacs G. Scaffold-free vascular tissue engineering using bioprinting. Biomaterials. 2009; 30:5910–5917. [PubMed: 19664819]
5. Seliktar D, Dikovsky D, Napadensky E. Bioprinting and tissue engineering: recent advances and future perspectives. Isr J Chem. 2013; 53:1–10.
6. Kim SS, Utsunomiya H, Koski Ja, Wu BM, Cima MJ, Sohn J, et al. Survival and function of hepatocytes on a novel three-dimensional synthetic biodegradable polymer scaffold with an intrinsic network of channels. Ann Surg. 1998; 228:8–13. [PubMed: 9671060]
7. Lin H-R, Yeh Y-J. Porous alginate/hydroxyapatite composite scaffolds for bone tissue engineering: preparation, characterization, and in vitro studies. J Biomed Mater Res Part B Appl Biomater. 2004; 71:52–65. [PubMed: 15368228]
8. Yao R, Zhang R, Luan J, Lin F. Alginate and alginate/gelatin microspheres for human adipose-derived stem cell encapsulation and differentiation. Biofabrication. 2012; 4:025007. [PubMed: 22556122]
9. Rowley JA, Madlambayan G, Mooney DJ. Alginate hydrogels as synthetic extracellular matrix materials. Biomaterials. 1999; 20:45–53. [PubMed: 9916770]
10. Nakamura M, Iwanaga S, Henmi C, Arai K, Nishiyama Y. Biomatrices and biomaterials for future developments of bioprinting and biofabrication. Biofabrication. 2010; 2:014110. [PubMed: 20811125]
11. Xu C, Chai W, Huang Y, Markwald RR. Scaffold-free inkjet printing of three-dimensional zigzag cellular tubes. Biotechnol Bioeng. 2012; 109:3152–3160. [PubMed: 22767299]
12. Billiet T, Vandenhaute M, Schelfhout J, Van Vlierberghe S, Dubruel P. A review of trends and limitations in hydrogel-rapid prototyping for tissue engineering. Biomaterials. 2012; 33:6020–6041. [PubMed: 22681979]

13. Lewis KJR, Anseth KS. Hydrogel scaffolds to study cell biology in four dimensions. MRS Bull. 2013; 38:260–268. [PubMed: 25221384]
14. Badylak SF. The extracellular matrix as a scaffold for tissue reconstruction. Cell Dev Biol. 2002; 13:377–383.
15. Kim B-S, Mooney DJ. Development of biocompatible synthetic extracellular matrices for tissue engineering. Trends Biotechnol. 1998; 16:224–230. [PubMed: 9621462]
16. Orive G, Carcaboso AM, Hernández AM, Gascón AR, Pedraz JL. Biocompatibility evaluation of different alginates and alginate-based microcapsules. Biomacromolecules. 2005; 6:927–931. [PubMed: 15762661]
17. Al-shamkhani A, Duncan R. Radioiodination of alginate via covalently-bound tyrosinamide allows monitoring of its fate in vivo. J Bioact Compat Polym. 1995; 10:4–13.
18. Lee M, Wu BM. Recent Advances in 3D printing of Tissue Engineering Scaffols. Comput Tissue Eng. 2012:257–267. [cited 2013 May 22].
19. Wang L, Shansky J, Borselli C, Mooney D, Vandenburgh H. Design and fabrication of a biodegradable, covalently crosslinked shape-memory alginate scaffold for cell and growth factor delivery. Tissue Eng Part A. 2012; 18:2000–2007. [PubMed: 22646518]
20. Bouhadir KH, Lee KY, Alsberg E, Damm KL, Anderson KW, Mooney DJ. Degradation of partially oxidized alginate and its potential application for tissue engineering. Biotechnol Prog. 2001; 17:945–950. [PubMed: 11587588]
21. Lee KY, Mooney DJ. Alginate: properties and biomedical applications. Prog Polym Sci. 2012; 37:106–126. [PubMed: 22125349]
22. Murphy SV, Skardal A, Atala A. Evaluation of hydrogels for bio-printing applications. J Biomed Mater Res A. 2013; 101:272–284. [PubMed: 22941807]
23. Chung JHY, Naficy S, Yue Z, Kapsa R, Quigley A, Moulton SE, et al. Bio-ink properties and printability for extrusion printing living cells. Biomater Sci. 2013; 1:763.
24. Gimble JM, Katz AJ, Bunnell BA. Adipose-derived stem cells for regenerative medicine. Circ Res. 2007; 100:1249–1260. [PubMed: 17495232]
25. Pataky K, Braschler T, Negro A, Renaud P, Lutolf MP, Brugger J. Microdrop printing of hydrogel bioinks into 3D tissue-like geometries. Adv Mater. 2011; 24:391–396. [PubMed: 22161949]
26. Alsberg E, Anderson KW, Albeiruti A, Rowley JA, Mooney DJ. Engineering growing tissues. Proc Natl Acad Sci U S A. 2002; 99:12025–12030. [PubMed: 12218178]
27. Boontheekul T, Kong H-J, Mooney DJ. Controlling alginate gel degradation utilizing partial oxidation and bimodal molecular weight distribution. Biomaterials. 2005; 26:2455–2465. [PubMed: 15585248]
28. Malda J, Visser J, Melchels FP, Jüngst T, Hennink WE, Dhert WJA, et al. 25th Anniversary Article: Engineering Hydrogels for Biofabrication. Adv Mater. 2013:1–18.
29. Derby B. Printing and prototyping of tissues and scaffolds. Science (80-). 2012; 338:921–926.
30. Ferris CJ, Gilmore KG, Wallace GG, In het Panhuis M. Biofabrication: an overview of the approaches used for printing of living cells. Appl Microbiol Biotechnol. 2013; 97:4243–4258. [PubMed: 23525900]
31. Blaeser A, Duarte Campos DF, Weber M, Neuss S, Theek B, Fischer H, et al. Biofabrication under fluorocarbon: a novel freeform fabrication technique to generate high aspect ratio tissue-engineered constructs. Biores Open Access. 2013; 2:374–384. [PubMed: 24083093]
32. Maher PS, Keatch RP, Donnelly K, Mackay RE, Paxton JZ. Construction of 3D biological matrices using rapid prototyping technology. Rapid Prototyp J. 2009; 15:204–210.
33. Gaetani R, Doevendans PA, Metz CHG, Alblas J, Messina E, Giacomello A, et al. Cardiac tissue engineering using tissue printing technology and human cardiac progenitor cells. Biomaterials. 2012; 33:1782–1790. [PubMed: 22136718]
34. Guillotin B, Souquet A, Catros S, Duocastella M, Pippenger B, Bellance S, et al. Laser assisted bioprinting of engineered tissue with high cell density and microscale organization. Biomaterials. 2010; 31:7250–7256. [PubMed: 20580082]

35. Lin H, Zhang D, Alexander PG, Yang G, Tan J, Cheng AW-M, et al. Application of visible light-based projection stereolithography for live cell-scaffold fabrication with designed architecture. Biomaterials. 2013; 34:331–339. [PubMed: 23092861]
36. Schuurman O, Levett PA, Pot MW, Weeren PR, van Dhert WJA, Hutmacher DW, et al. Gelatin-Methacrylamide Hydrogels as Potential Biomaterials for Fabrication of Tissue-Engineered Cartilage Constructs. Macromol Biosci. 2013; 13:551–561. [PubMed: 23420700]
37. Fedorovich NE, De Wijn JR, Verbout AJ, Alblas J, Dhert WJA. Three-dimensional fiber deposition of cell-laden, viable, patterned constructs for bone tissue printing. Tissue Eng Part A. 2008; 14:127–133. [PubMed: 18333811]
38. Fedorovich NE, Schuurman W, Wijnberg HM, Prins H-J, van Weeren PR, Malda J, et al. Biofabrication of Osteochondral Tissue Equivalents by Printing Topologically Defined, Cell-Laden Hydrogel Scaffolds. Tissue Eng Part C Methods. 2012; 18:33–44. [PubMed: 21854293]
39. Tirella A, Orsini A, Vozzi G, Ahluwalia A. A phase diagram for microfabrication of geometrically controlled hydrogel scaffolds. Biofabrication. 2009; 1:045002. [PubMed: 20811111]
40. Bryant SJ, Anseth KS. Hydrogel properties influence ECM production by chondrocytes photoencapsulated in poly(ethylene glycol) hydrogels. J Biomed Mater Res. 2002; 59:63–72. [PubMed: 11745538]
41. Nicodemus GD, Bryant SJ. Review: Cell encapsulation in biodegradable hydrogels for tissue engineering applications. Tissue Eng Part B. 2008; 14:149–165.
42. Kong HJ, Kaigler D, Kim K, Mooney DJ. Controlling rigidity and degradation of alginate hydrogels via molecular weight distribution. Biomacromolecules. 2004; 5:1720–1727. [PubMed: 15360280]
43. Kang KH, Hockaday LA, Butcher JT. Quantitative optimization of solid freeform deposition of aqueous hydrogels. Biofabrication. 2013; 5:035001. [PubMed: 23636927]
44. Tholpady SS, Aojanepong C, Llull R, Jeong J-H, Mason AC, Futrell JW, et al. The Cellular Plasticity of Human Adipocytes. Ann Plast Surg. 2005; 54:651–656. [PubMed: 15900154]
45. Spiegelman BM, Ginty CA. Fibronectin modulation of cell shape and lipogenic gene expression in 3T3-adipocytes. Cell. 1983; 35:657–666. [PubMed: 6686086]
46. McBeath R, Pirone DM, Nelson CM, Bhadriraju K, Chen CS. Cell shape, cytoskeletal tension, and RhoA regulate stem cell lineage commitment. Dev Cell. 2004; 6:483–495. [PubMed: 15068789]
47. Ruoslahti E. RGD and other recognition sequences for integrins. Annu Rev Cell Dev Biol. 1996; 12:697–715. [PubMed: 8970741]
48. D'Souza SE, Ginsberg MHPE. Arginyl-glycyl-aspartic acid (RGD): a cell adhesion motif. Trends Biochem Sci. 1991; 16:246–250. [PubMed: 1926332]
49. Pfaff M, Tangemanno K, Mullero B, Gurrathnll M, Miillerll G, Kesslern H, et al. Selective Recognition of Cyclic RGD Peptides of NRlR Defined. J Biol Chem. 1994; 269:20233–20238. [PubMed: 8051114]
50. Zuk PA, Zhu M, Ashjian P, Ugarte DA, De Huang JI, Mizuno H, et al. Human Adipose Tissue Is a Source of Multipotent Stem Cells. Mol Biol Cell. 2002; 13:4279–4295. [PubMed: 12475952]
51. Zuk PA, Zhu M, Mizuno H, Huang J, Futrell JW, Katz AJ, et al. Multilineage cells from human adipose tissue: implications for cell-based therapies. Tissue Eng. 2001; 7:211–228. [PubMed: 11304456]
52. Zhu Y, Liu T, Song K, Fan X, Ma X, Cui Z. Adipose-derived stem cell: a better stem cell than BMSC. Cell Biochem Funct. 2008; 26:664–675. [PubMed: 18636461]
53. Matsuoka F, Takeuchi I, Agata H, Kagami H, Shiono H, Kiyota Y, et al. Morphology-based prediction of osteogenic differentiation potential of human mesenchymal stem cells. PLoS One. 2013; 8:e55082. [PubMed: 23437049]
54. Häuselmann HJ, Fernandes RJ, Mok SS, Schmid TM, Block JA, Aydelotte MB, et al. Phenotypic stability of bovine articular chondrocytes after long-term culture in alginate beads. J Cell Sci. 1994; 107:17–27. [PubMed: 8175906]
55. Stains JP, Civitelli R. Cell-cell interactions in regulating osteogenesis and osteoblast function. Birth Defects Res C Embryo Today. 2005; 75:72–80. [PubMed: 15838921]

56. Benton JA, Fairbanks BD, Anseth KS. Characterization of valvular interstitial cell function in three dimensional matrix metalloproteinase degradable PEG hydrogels. Biomaterials. 2009; 30:6593–6603. [PubMed: 19747725]

57. Yellowley CE, Hancox JC, Donahue HJ. Effects of cell swelling on intracellular calcium and membrane currents in bovine articular chondrocytes. J Cell Biochem. 2002; 86:290–301. [PubMed: 12111998]

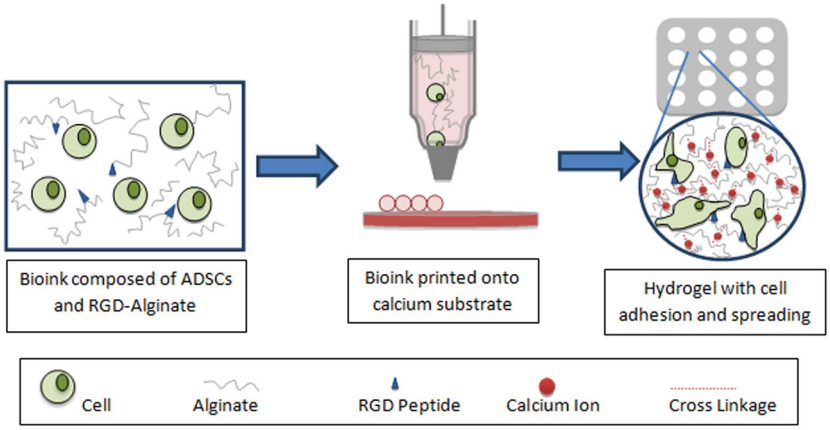

Figure 1.

Schematic representation of biodegradable oxidized alginate as bioink for bioprinting. A bioink consisting of RGD-modified oxidized alginate hADSCs was printed in a define lattice structure on a gelatin substrate to crosslink the hydrogel. The constructs were then evaluated over an 8-day period for cellular behavior (i.e., cell proliferation and spreading).

a)

Density(g/cm^3)						
Conc. / Ox.	2	5	8	10	15	20
0	1.01 ± 0.003	1.04 ± 0.009	1.07 ± 0.012	1.09 ± 0.029	-	-
1	1.01 ± 0.008	1.03 ± 0.015	1.07 ± 0.017	1.12 ± 0.032	-	-
3	1.01 ± 0.005	1.03 ± 0.008	1.06 ± 0.016	1.08 ± 0.006	1.15 ± 0.032	-
5	1.01 ± 0.008	1.02 ± 0.009	1.04 ± 0.009	1.05 ± 0.006	1.12 ± 0.008	1.15 ± 0.031
10	1.01 ± 0.008	1.01 ± 0.013	1.04 ± 0.013	1.04 ± 0.011	1.08 ± 0.020	1.12 ± 0.017

b)

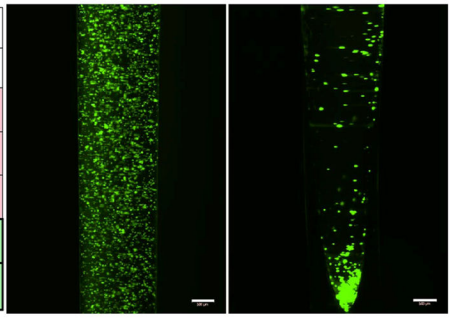

Figure 2.

Density-based analysis on printability of different alginate solutions. (a) Density (mean ± SD) measurements of each sample with successful cell suspension results (green). Red denotes alginate compositions that did not completely dissolve into solution after 2 days. The other materials (white) were unable to maintain a homogenous cell distribution. (b) Calcein-stained hADSCs in the 5% ox.-10% conc. (left) and 5% ox.-2% conc. (right) material with and without successful cell suspension, respectively (scale bar= 500 μm).

a)

Kinetic Viscosity(mm^2/s)						
Conc. / Ox.	2	5	8	10	15	20
0	34.85 ± 1.01	523.63 ± 19.7	2202.7 ± 748	3390.4 ± 568	-	-
1	19.15 ± 0.25	201.8± 11.3	702.78 ± 7.15	2793.1 1± 204	-	-
3	13.4± 1.01	82.3± 5.56	352.9± 9.66	1414.1 ± 12.9	>8000	-
5	9.5± 0.75	57.4± 8.50	210.9± 8.06	701± 25.9	1034± 23.0	>8000
10	4.5± 0.16	11.8± 0.52	29.5± 0.71	58.1± 2.61	457.6 ± 13.3	2750± 396

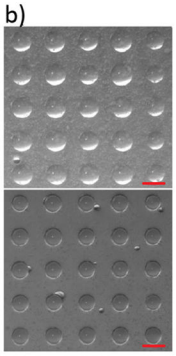

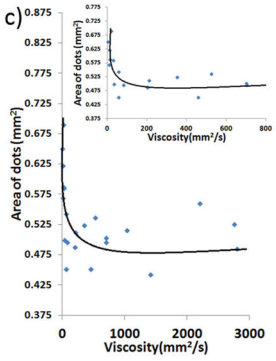

Figure 3.

Viscosity-based analysis on printability of different alginate solutions. (a) Viscosity values of various alginate solutions with a range of concentrations and oxidation levels that passed the density requirement shown with a favorable area for higher resolution bioprinting with hADSCs (green). Red denotes alginate compositions that did not completely dissolved into solution after 2 days. The other materials were either too viscous to prepare for printing or failed the density test (white). (b) Using dots as the functional unit of liquid-dispensing strategies and a representation of resolution, a printed dot array (5×5) shows examples of low printing resolution (top), high printing resolution (low) (scale bar= 1 mm). (c) A plot of areas of dots versus viscosity shows a direct relationship between printability and viscosity of alginate samples. Guiding lines represent general flow of data.

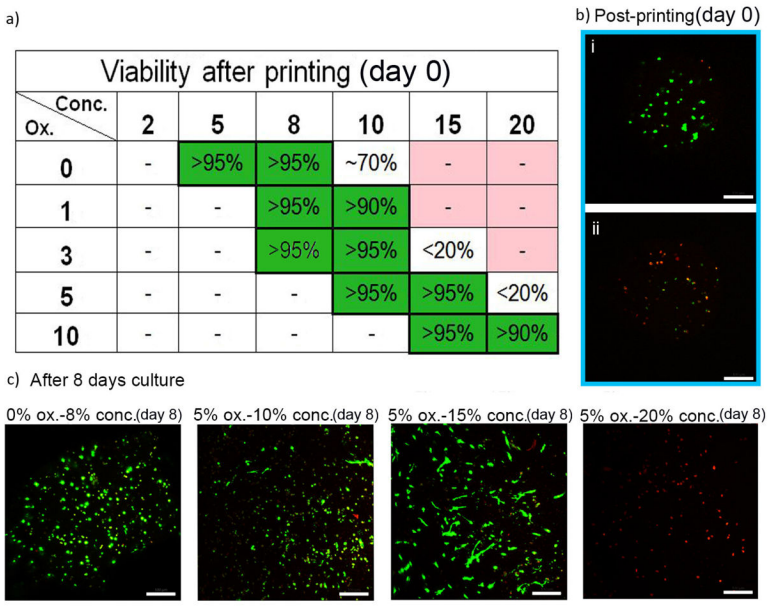

Figure 4.

Cell viability assay of density and viscosity criterion-filtered samples. (a) Samples of high viability (>90%) right after printing (green). (b) The fluorescent pictures of live-dead assay after printing: (i) high cell viability sample (e.g. 5% ox.-15% conc.) and (ii) low cell viability sample (e.g. 5% ox.-20% conc.) (scale bar= 100 μm). (c) Cell viability assay at day 8. Except the 5% ox.-20% conc. sample (0% viability), the remaining four samples showed high viabilities (>95%) after 8 days in culture (scale bar= 100 μm).

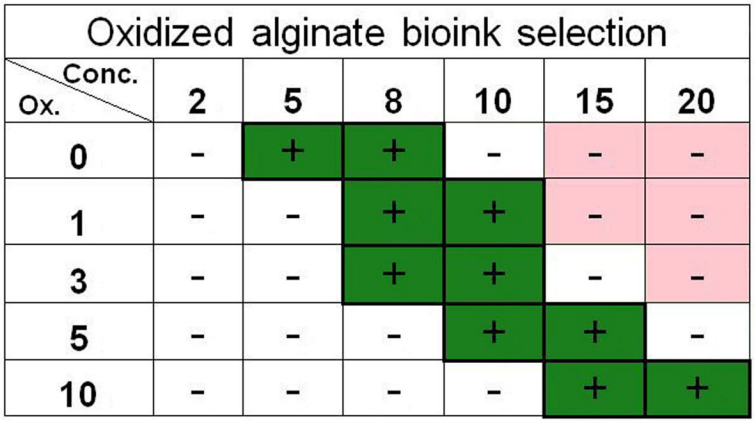

Figure 5.

Summary table of the preferable range of alginate samples with high printability (green) based on the three established printability criteria (i.e., homogeneous cell suspension, high printing resolution, and high cell viability).

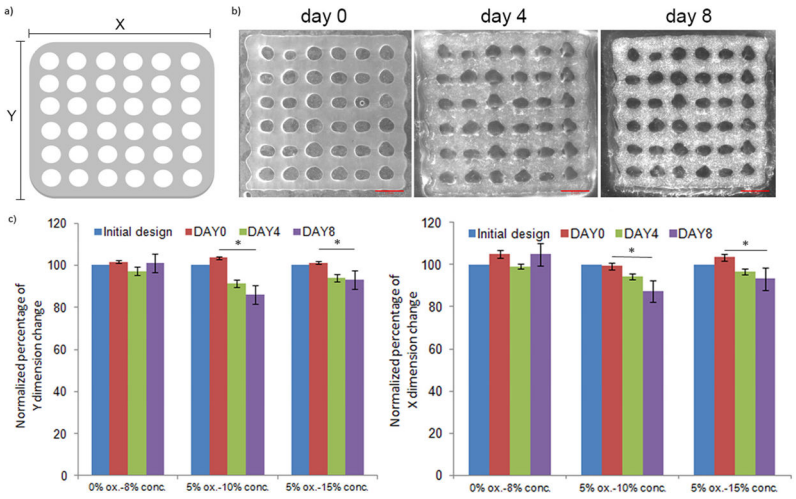

Figure 6.

Lattice structures printed with bioprinting-compatible materials and their dimensional change in 8 days. (a) Initial design of lattice structure. (b) Pictures of printed lattice structures (5% ox.-10% conc. sample) at day 0, day 4, day 8 shows printed structures highly matched the initial design with apparent dimensional changes after 8 days in culture (scale bar= 2 mm). (c) Normalized comparison between the initial design (12.6 mm × 12.6 mm) and the X and Y dimensions of the lattice structures (0% ox.-8% conc., 5% ox.-10% conc., 5% ox.-15% conc.) after 8 days in culture. All values are mean ± SD. Asterisk denotes significant difference between day 0 and day 8.

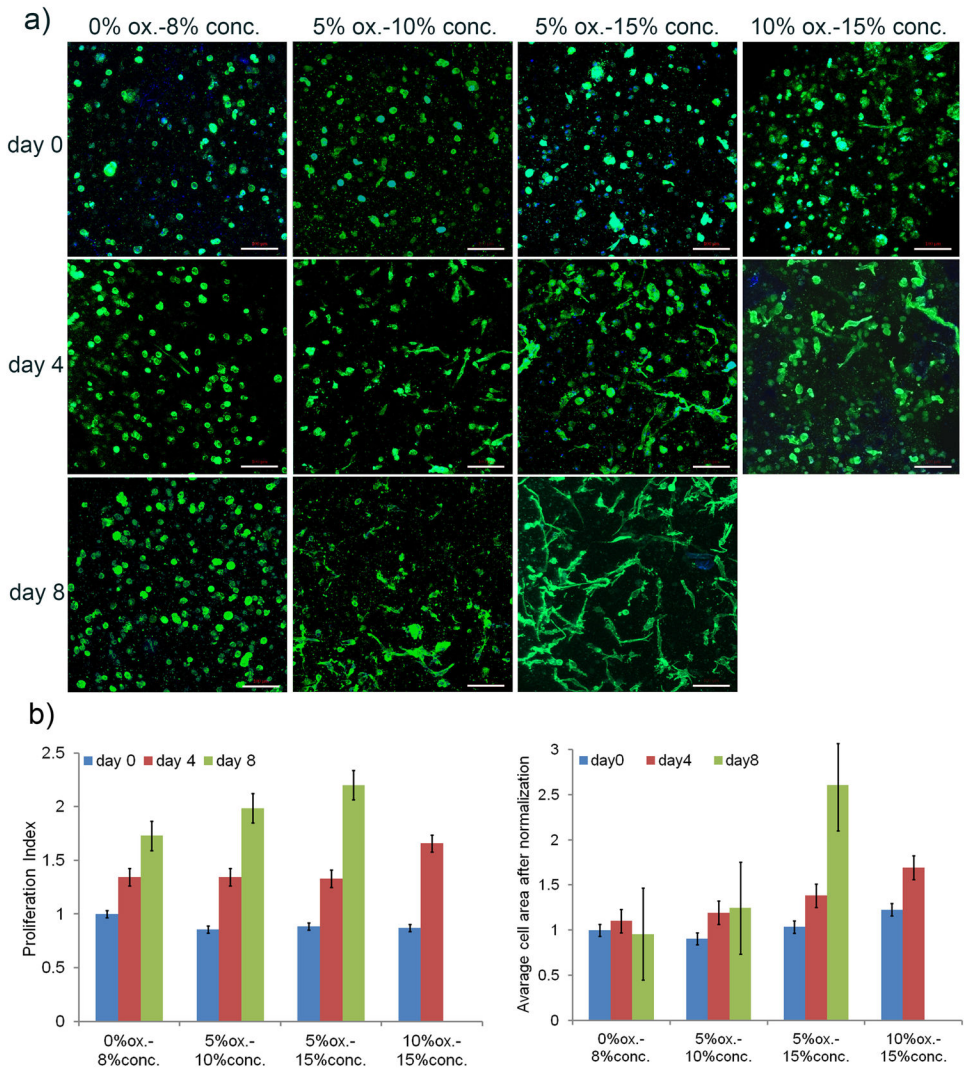

Figure 7.

hADSC behavior in the lattice structures. (a) Cell spreading with fluorescent staining (phalloidin) for actin at day 0, 4, and 8 (scale bar= 100 μm). (b) hADSC proliferation index and spreading assays based on fluorescent staining (phalloidin and DAPI stain) at day 8. Proliferation index was calculated as the cell number of each day divided by the original cell number on day 0 for the 0% ox.-8% conc. alginate sample for relative comparison. Cell area was calculated as total cell area divided by the number of cells normalized over the values at day 0 for the 0% ox.-8% conc. alginate sample. All values are mean ± SD.

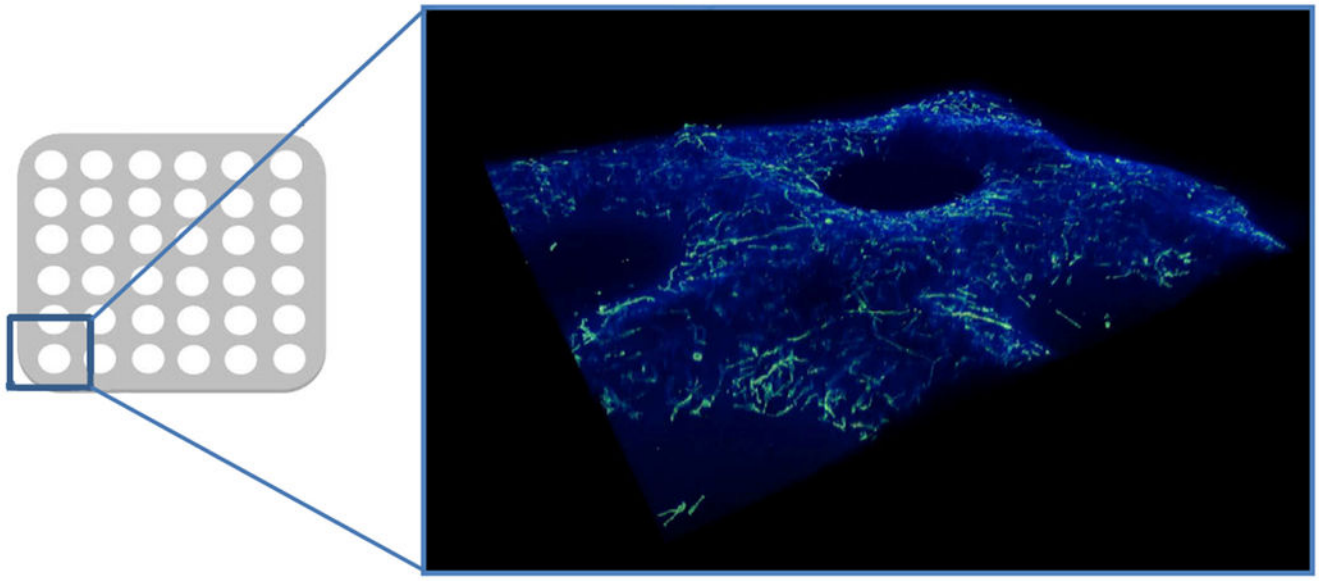

Figure 8.

A computer-rendered 3D picture of a portion of the printed lattice structure made by the best supporting hADSC material, 5% ox.-15% conc. oxidized alginate, showing multiple layers of spreading cells within the hydrogel.